Available online at www.eccomasproceedia.org
Eccomas Proceedia COMPDYN (2025) 1193-1200

ECCOMAS
Proceedia

COMPDYN 2025
10th ECCOMAS Thematic Conference on
Computational Methods in Structural Dynamics and Earthquake Engineering
M. Papadrakakis, M. Fragiadakis (eds.)
Rhodes Island, Greece, 15-18 June 2025

HIGH CONTRAST BIPHASIC MECHANICAL METAMATERIALS FOR THE MITIGATION OF ELASTIC WAVE PROPAGATION

Meng Wang[1], Annamaria Pau[1], Marco Lepidi[2], and Luigi Martirano[1]

[1]Sapienza Università di Roma
via Eudossiana 18, 00184, Roma, Italy
meng.wang@uniroma1.it, annamaria.pau@uniroma1.it, luigi.martirano@uniroma1.it

[2] Università degli Studi di Genova
Via Montallegro 1, 16145, Genova, Italy
marco.lepidi@unige.it

Abstract. *This paper reports investigations on two-dimensional phononic crystals composed of two distinct material phases. Focus is on the undamped free propagation of elastic harmonic waves in high-contrast linear elastic materials, whereby the effects of topology and contrast rate of component phases are studied. Solid-solid biphasic mechanical metamaterials are composed of alternating solid phases with significant difference in material properties. Stop bandwidths depend on the contrast between the material properties of the inclusions and the matrix, as well as on the geometry of the array of inclusions and the inclusion shape. The SAFE method provides an analytical framework to compute dispersion relations: a tentative solution representing plane waves is substituted in the equations of motion, then periodicity conditions are applied on the boundary of the repetitive cell, providing an eigenvalue problem. Parametric and topological design has demonstrated the potential to achieve ultra-wide bandgaps in solid-solid phononic crystals within the frequency range of human sensitivity.*

Keywords: Periodic Materials, Biphasic Phononic Crystals, High Contrast Materials, SAFE Method, Spectra Design.

ISSN:2623-3347 © 2025 The Authors. Published by Eccomas Proceedia.
Peer-review under responsibility of the organizing committee of COMPDYN 2025.
doi: 10.7712/120125.12482.25874

1 INTRODUCTION

Propagation of elastic waves in phononic crystals has garnered significant attention in the last decades. These materials are heterogeneous engineered media, or metamaterials, typically consisting of periodic arrays of inclusions embedded within a base matrix. By virtue of Bragg scattering mechanisms, these metamaterials often show bandgaps in their dispersion spectra, which inhibit the free propagation of elastic vibrations. Consequently, the primary focus in the design of artificial metamaterials as phononic crystals lies in bandgap engineering, aiming to achieve wide bandgaps within target frequency ranges, facilitating the development of metadevices with tailored dynamic responses for advanced functional applications [1].

Solid-solid biphasic mechanical metamaterials, composed of alternating solid phases with significant differences in material properties, exhibit unique capabilities for controlling elastic wave propagation. Earlier studies have shown that the formation of wide bandgaps in phononic crystals necessitates: (i) significant contrasts in physical properties, such as density and elastic moduli, between the inclusions and the matrix, and (ii) an adequate inclusion filling factor [2, 3].

The dispersion characteristics of phononic crystals are strongly affected by the geometric arrangement of their constituent materials. This evidence has led to increasing interest in spatial distribution optimization, as a suitable alternative to microstructural design [4]. Specifically, topology optimization driven by genetic algorithms [5, 6] has demonstrated the potential to achieve ultra-wide bandgaps in solid-solid phononic crystals. Among these research findings, the majority of studies targeted at the maximization of bandgap widths have consistently highlighted the critical role of intra-phase connectivity in spatial topology, that is, the introduction of inter-inclusion “channels” as a crucial design variable [7].

Building on previous research, this study focuses on the distinction between the presence and absence of spatial connectivity. By examining the interplay between material contrast and spatial topology in solid–solid phononic crystals, the paper aims to identify the unexplored conditions that enable the opening of wide bandgaps through the combined influence of interphase contrast and intra-phase connectivity, specifically within the frequency range of human sensitivity to elastoacoustic vibrations [8]. The geometric configurations of the repetitive cell and its periodic arrangements are described in Section 2. The dispersion properties governing the free wave propagation are obtained by semi-analytical finite element method in Section 3. Parametric analyses exploring how the amplitude of bandgaps varies under two topological alternatives, with and without spatial connectivity, are presented in Section 4.

2 BIPHASIC SOLID-SOLID PHONONIC CRYSTAL

A two-dimensional phononic crystal is investigated, consisting of an infinitely repeated periodic cell with square shape (Figure 1a). The periodic pattern is described by a pair of orthogonal vectors, $\mathbf{a}_1$ and $\mathbf{a}_2$, which define the geometric periodicity in the planar space. The periodic cell exhibits a biphasic topology with double symmetry (Figure 1b), where the base matrix (phase $\mathcal{A}_{\mathrm{I}}$, shown in gray) embeds a centered circular inclusion (phase $\mathcal{A}_{\mathrm{II}}$, indicated in light blue). This topology can be further enriched by introducing microstructural features. In this study, straight channels, collinear to the periodicity vectors and connecting the inclusions of neighboring cells are used to introduce intra-phase connectivity between adjacent cells (Figure 1c). The channel opening preserves the double symmetry of the cell. The geometric configuration of the phononic crystal is entirely defined by the side length of the periodic cell, $L = |\mathbf{a}_1| = |\mathbf{a}_2|$, the radius of the circular inclusion r and the width of the connecting channels w.

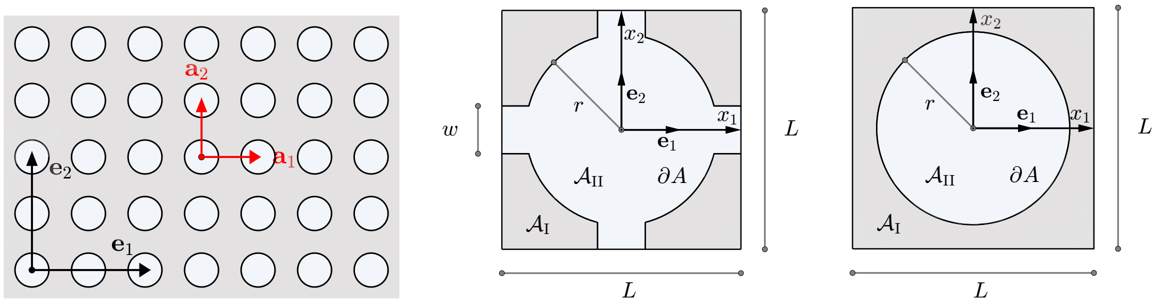

(a) (b) (c)

Figure 1: Sketch of the periodic biphasic metamaterial: (a) periodic planar pattern, (b) repetitive cell with channels, (c) repetitive cell without channels.

3 GOVERNING EQUATIONS

Solid phases consist of linear elastic, homogeneous, non-dissipative, and isotropic materials. The dynamic behavior is described by a state of plane strain, represented by the displacement vector field $\mathbf{u} = (u_1, u_2)^\top$, which depends on time t and spatial position $\mathbf{x} = (x_1, x_2)^\top$, spanning the plane defined by the basis vectors $\mathbf{e}_1 - \mathbf{e}_2$. According to the classical Cauchy formulation, the governing field equations are

$$\mu^j \Delta \mathbf{u}^j + (\lambda^j + \mu^j)\nabla \mathrm{div}\mathbf{u}^j = \rho^j \ddot{\mathbf{u}}^j \quad \text{on} \quad \mathcal{A}_j \tag{1}$$

where the index j =I,II denotes the two different solid phases, λ^j and μ^j are the Lamé constants, and ρ^j is the material density. Moreover, $\nabla = (\partial/\partial x_1, \partial/\partial x_2)^\top$, $\Delta = \nabla \cdot \nabla$, and the double dots indicate the second derivative with respect to time t. The boundary conditions on the region between phases enforce the continuity of displacements and the balance of normal tractions

$$\mathbf{u}^{\mathrm{I}} = \mathbf{u}^{\mathrm{II}}, \quad \boldsymbol{\sigma}^{\mathrm{I}} \cdot \mathbf{n} = \boldsymbol{\sigma}^{\mathrm{II}} \cdot \mathbf{n} \quad \text{on} \quad \partial\mathcal{A} \tag{2}$$

where $\boldsymbol{\sigma}$ is the stress tensor and $\mathbf{n}$ is the versor normal to $\partial\mathcal{A}$.

3.1 Semi-analytical finite element (SAFE) method

From a methodological point of view, the solutions are derived using an analytical-numerical approach, which builds upon the classical semi-analytical finite element (SAFE) method [9, 10]. Free dynamic solutions are represented by waves that oscillate harmonically in time with a real-valued angular frequency ω and propagate periodically through space, with a plane wavefront orthogonal to the real-valued wavevector $\mathbf{k} = (k_1, k_2)^\top$, reading

$$\mathbf{u}(\mathbf{x}, t) = \mathbf{U}(\mathbf{x})\mathrm{e}^{\mathrm{i}(\mathbf{k}\cdot\mathbf{x} - \omega t)} \tag{3}$$

where i is the imaginary unit, and the vector field $\mathbf{U}(\mathbf{x}) = (U_1, U_2)^\top$ represents the time-independent waveform, which parametrically depends on the wavevector.

Without resorting to Floquet boundary conditions, here the analysis is conducted by enforcing general periodic conditions on the two pairs of boundaries: horizontal (top and bottom) and vertical (left and right). This approach gives rise to a parametric eigenproblem, where ω^2 and $\mathbf{U}$ play the role of the eigenvalue and eigenvector, respectively, depending on the parameter $\mathbf{k}$. Originating from the topology of a base matrix with a centered circular inclusion, both cases

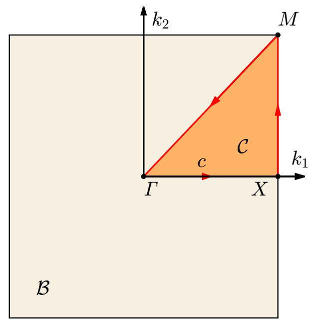

Figure 2: First Brillouin zone $\mathcal{B}$, irreducible Brillouin zone $\mathcal{C}$ and reduced wavevector $c : \Gamma \to X \to M \to \Gamma$.

— with and without channels — are considered. The eigenproblem is solved within the finite cellular domain $\mathcal{A}_{\mathrm{I}} \cup \mathcal{A}_{\mathrm{II}}$ of the periodic cell, while the wavevector $\mathbf{k}$ spans the square first Brillouin zone $\mathcal{B} = [-\pi/L, \pi/L] \times [-\pi/L, \pi/L]$ (Figure 2). From the computational viewpoint, the analysis can be efficiently reduced to the Irreducible Brillouin Contour, which serves as a computationally cost-effective alternative. This contour corresponds to the closed boundary $\partial\mathcal{C}$ of the triangular Irreducible Brillouin Zone $\mathcal{C} \subset \mathcal{B}$, identified by the three vertices $\Gamma = (0, 0)$, $X = (\pi/L, 0)$, $M = (\pi/L, \pi/L)$. The closed boundary $\partial\mathcal{C}$ is spanned by the curvilinear abscissa $c \in [0, (2 + \sqrt{2})\pi/L]$, known as the *reduced wavevector*. Physically, all the frequency ranges included in the codomain of the real-valued dispersion function $f(c) = \omega(c)/2\pi$, correspond to passbands, in which harmonic waves can freely propagate. Complementarily, frequency ranges excluded from the codomain of the real value of $f(c)$ correspond to complete stopbands or bandgaps, in which propagation of harmonic waves is inhibited.

4 SPECTRAL DESIGN FOR WAVE ATTENUATION

4.1 Dispersion spectra and bandgap

The curves mapping the dispersion function in the plane spanned by frequency (vertical coordinate) and reduced wavevector (horizontal coordinate) are branches of the dispersion diagram. The eigenvalue problem is computationally solved by finite element techniques implemented in COMSOL using the PDE module in coefficient form. A sample of the obtained numerical dispersion diagrams is reported in Figure 3. The geometric properties are: side length $L = 30$ mm, inclusion radius $r = 12$ mm, and channel width $w = 6$ mm. Nylon and Aluminum are chosen as materials of the two phases, with mechanical properties detailed in Table 1. Only the configuration with Aluminum matrix with Nylon inclusion is presented in Figure 3 for the sake of brevity. Similar results were obtained by exchanging the two material phases.

The dispersion curves of Figure 3 exhibit a strong frequency dependence on the reduced wavevector c. The stop and pass bands are indicated by a red and green background, respectively, in the diagrams. Additionally, the normalized frequency, defined as $f^* = f \cdot L/v$, with v shear bulk wave velocity, is added on the right hand side of the diagram. This quantity facilitates comparative analysis across different topologies and scalable cell design with consistent bandgap characteristics. It is apparent that the configuration with connecting channels presents a wide bandgap in the frequency range of interest between 0.8 and 1.5 f^*.

Material	Density	Modulus of Elasticity	Poisson's Ratio	Transverse Velocity
Nylon	1000 kg/m^3	1.75 GPa	0.34	811 m/s
Aluminum	2700 kg/m^3	69 GPa	0.33	3043 m/s

Table 1: Mechanical properties of the distinct phases.

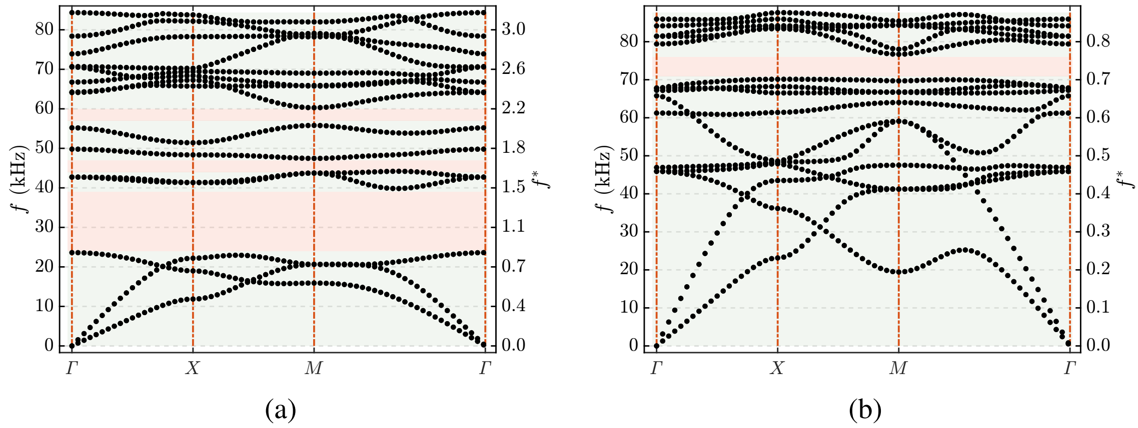

Figure 3: Dispersion diagrams for Aluminum matrix with Nylon inclusions: (a) in the presence of channels, and (b) in the absence of channels.

4.2 Parametric analysis

The contrast between the constitutive properties of the two solid phases (matrix and inclusion) is chosen as design variable, whereas the largest normalized width of the lowest bandgap is selected as design target. The acoustic impedance is defined as $Z = v\rho$, that is the product between the shear bulk wave velocity and the density. The material contrast is defined by the impedance ratio ($Z_{\text{in}}/Z_{\text{base}}$) of the inclusion and of the matrix material. To check how the material contrast modifies the band structure, parametric analyses of the dispersion diagram are carried out by fixing the material of the base matrix (Nylon or Aluminium) and varying the material of the inclusion. Specifically, the impedance ratio $Z_{\text{in}}/Z_{\text{base}}$ is varied by simultaneously adjusting the elastic modulus and density of the inclusion, while keeping the base matrix properties fixed. The impedance of the inclusion spans a wide interval, ranging from values significantly lower than the base matrix ($Z_{\text{in}}/Z_{\text{base}} = 0.1$) to values considerably higher ($Z_{\text{in}}/Z_{\text{base}} = 10$). The range of material impendances investigated is very large, as the primary objective is to establish a general understanding of how the material contrast influences bandgap formation across different geometric configurations. Therefore, high constrast biphasic metamaterials are found at the limiting values of the exploration range.

Figures 4 and 5 present the dispersion curves in the presence and in the absence of channels, respectively, for selected values of the material contrast and fixed Nylon matrix. The case of Aluminum matrix produces similar outcomes and is not reported for the sake of brevity. Figure 6 illustrates the normalized bandgap widths $\Delta f/f_{\text{m}}$ determined over a more refined range of contrast values. Numerator The Δf is the difference between the upper and lower frequency boundaries of a bandgap, while denominator f_{m} is the central frequency of each bandgap, which is defined as the mean value of the upper and lower frequency boundaries.

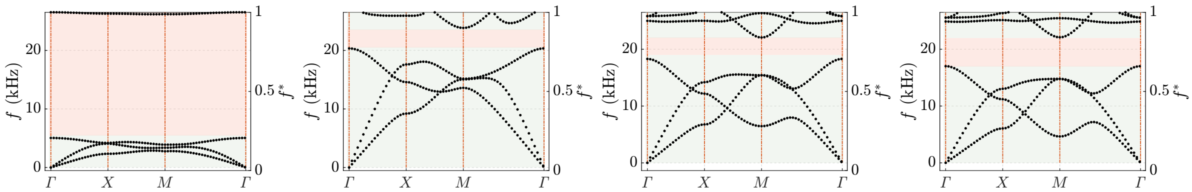

(a) (b) (c) (d)

Figure 4: Dispersion diagram for the case with Nylon as the base matrix, the values for impedance ratio of inclusion with channels are (a) 0.1, (b) 0.5, (c) 5, (d) 10.

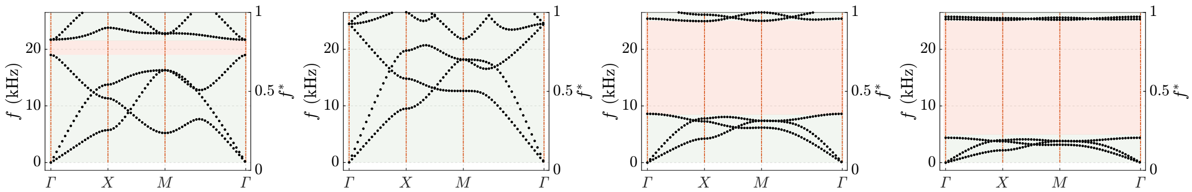

(a) (b) (c) (d)

Figure 5: Dispersion diagram for the case with Nylon as the base matrix, the values for impedance ratio of inclusion without channels are (a) 0.1, (b) 0.5, (c) 5, (d) 10.

These results reveal that, regardless of whether channels are present or not, a significant contrast between the base matrix and the inclusion can potentially induce bandgaps at both high and low acoustic impedance ratios. A more consistent trend is that wider bandgaps occur for lower value of $Z_{\mathrm{in}}/Z_{\mathrm{base}}$ in the configuration with channels. Opposite to that, for the configuration without channels, higher values of $Z_{\mathrm{in}}/Z_{\mathrm{base}}$ tend to produce broader bandgaps. This distinction highlights the strong influence of changes in the geometric topology, in particular the introduction of intra-phase channels, on the formation of bandgaps.

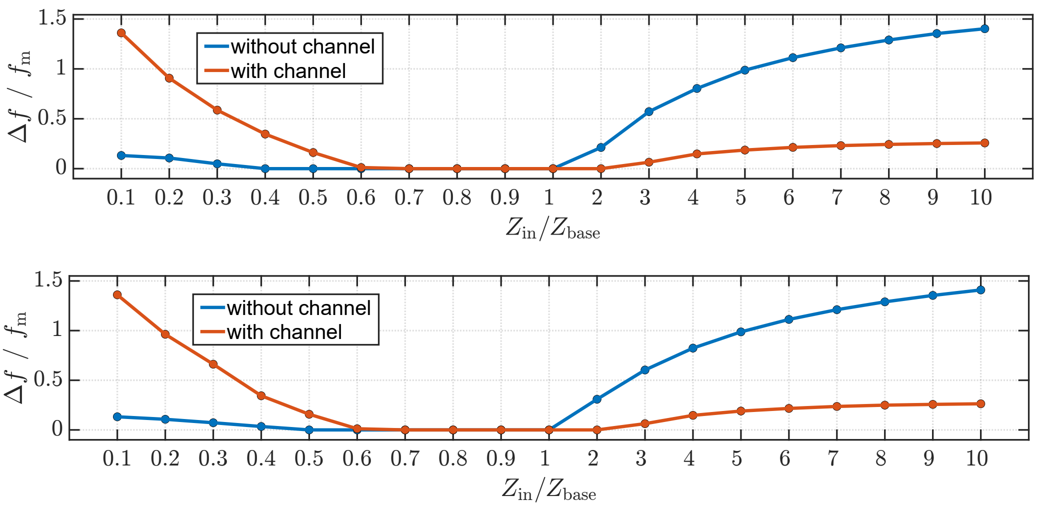

Figure 6: Variation of absolute stop bandwidth with $Z_{\mathrm{in}}/Z_{\mathrm{base}}$ when the base matrix is (a) Nylon and (b) Aluminum.

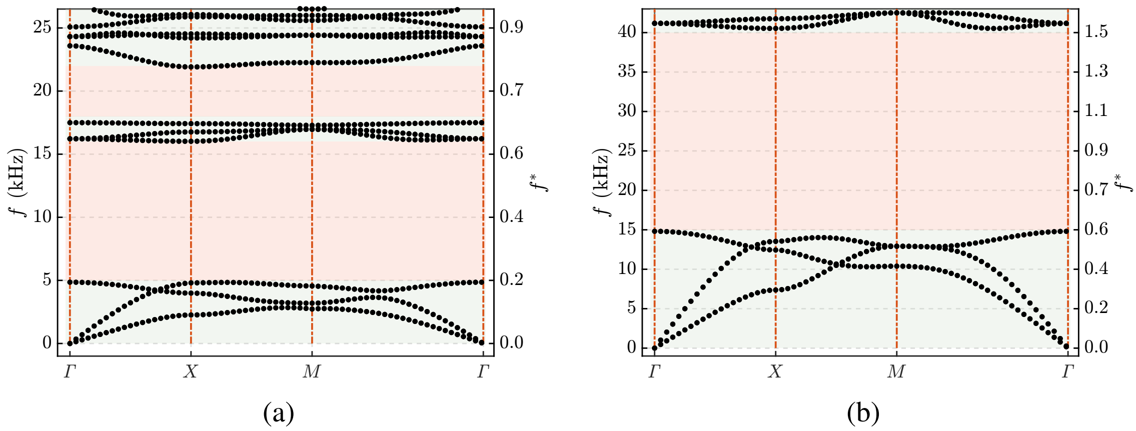

Figure 7: Dispersion diagrams of (a) configuration with channels made of Nylon and XPS Foam, and (b) configuration without channels made of Nylon with Steel.

4.3 Real high contrast materials combinations

The identified trends provide a useful guideline for the selection of practical material combinations to achieve broad bandgaps within the sensitivity frequency range under given geometric configurations. Following this approach, Nylon is used as the base matrix while XPS foam and steel were selected as inclusion materials for configurations with and without channels, respectively. The mechanical parameters are listed in Table 2. These materials were chosen as they represent more favorable options for achieving wide bandgaps under the corresponding geometric configurations. The dispersion diagrams in Figure 7 confirm that both cases successfully exhibit relatively broad bandgaps within the target frequency range.

5 CONCLUSIONS

This study investigates the influence of material contrast on the formation of bandgaps in two-dimensional solid-solid phononic crystals with periodic geometric configurations. The focus is placed on the comparison between two topological alternatives, that are configurations with and without channels connecting adjacent cells. The research findings reveal that the introduction of channels significantly alters the bandgap behavior compared to the absence of channels, resulting in opposite trends in bandgap formation across different contrast levels.

Specifically, in configurations without channels, increasing the impedance ratio between the matrix and inclusion tends to widen the bandgap, with the largest widths occurring at high impedance ratios. On the contrary, the introduction of channels leads to the opposite trend, where low impedance ratios enlarge the bandgap. These findings indicate that the presence of channels introduces additional waveguiding and scattering mechanisms that fundamentally alter the interaction between elastic waves and material phases.

Material	Density (ρ)	Modulus of Elasticity	Poisson's Ratio
Steel	8000 kg/m^3	193 GPa	0.29
XPS Foam	26 kg/m^3	24 MPa	0.35

Table 2: Mechanical properties of the high-contrast biphasic metamaterials.

These observations suggest that the topology of phononic crystals plays a crucial role in controlling the bandgap characteristics, beyond the material properties themselves. The opposite trends observed for configurations with and without channels provide valuable insights for the parametric design of phononic crystals, highlighting the importance of topology in mitigating elastic wave propagation within the frequency range of human sensitivity.

ACKNOWLEDGMENTS

This study was carried out within the MOST-Sustainable Mobility National Research Center. M.W. received funding from the European Union Next- GenerationEU (PIANO NAZIONALE DI RIPRESA E RESILIENZA (PNRR) - MISSIONE 4 COMPONENTE 2, INVESTIMENTO 1.4 - D.D. 1033 17/06/2022, CN00000023). A.P. acknowledges the funding contribution from the National Center on HPC, Big Data and Quantum Computing CN00000013 and from Sapienza grant No. 6023149. This manuscript reflects only the authors' views and opinions, neither the European Union nor the European Commission can be considered responsible for them.

REFERENCES

[1] Y. Pennec, J. Vasseur, B. Rouhani, L. Dobrzyński, P. Deymier, Two-dimensional phononic crystals: Examples and applications. *Surface Science Reports*, **65**, 229–291, 2010.

[2] J. Vasseur, P. A. Deymier, Absolute forbidden bands and waveguiding in two-dimensional phononic crystal plates. *Physical Review B*, **77**, 085415, 2008.

[3] O. R. Bilal, M. I. Hussein, Ultrawide phononic band gap for combined in-plane and out-of-plane waves. *Physical Review E*, **84**, 065701, 2011.

[4] F. Vadalà, A. Bacigalupo, M. Lepidi, L. Gambarotta. Bloch wave filtering in tetrachiral materials via mechanical tuning. *Composite Structures*, **201**, 340–351, 2018

[5] Y. Lu, Y. Yang, J. K. Guest, A. Srivastava, 3-D phononic crystals with ultra-wide band gaps. *Scientific Reports*, **7**, 43407, 2017.

[6] Z. Liu, B. Wu, C. He, Systematic topology optimization of solid–solid phononic crystals for multiple separate band-gaps with different polarizations. *Ultrasonics*, **65**, 249–257, 2016.

[7] Z. Jia, Y. Bao, Y. Luo, D. Wang, X. Zhang, Z. Kang. Maximizing acoustic band gap in phononic crystals via topology optimization. *International Journal of Mechanical Sciences*, **270**, 109107, 2024.

[8] M. Wang, A. Pau, M. Lepidi, Elastoacoustic wave propagation in a biphasic mechanical metamaterial. *Journal of Acoustical Society of America*, **155**, 3322–3335, 2024.

[9] A. Pau, F. Lanza di Scalea. Nonlinear guided wave propagation in prestressed plates. *Journal of Acoustical Society of America*, **137**, 1529–1540, 2015.

[10] A. Pau, P. Trovalusci. A multifield continuum model for the description of the response of microporous/microcracked composite materials. *Mechanics of Materials*, **160**, 103965, 2021.